IEEE Access
Multidisciplinary | Rapid Review | Open Access Journal

Received April 13, 2022, accepted April 25, 2022, date of publication April 29, 2022, date of current version May 6, 2022.

Digital Object Identifier 10.1109/ACCESS.2022.3171251

Inter-Signal Distortion Analysis in Multidimensional QAM-MDPSK Modulation Optical Access Transmissions

JOUNGMOON LEE, INHO HA, JINWOO PARK, AND SANG-KOOK HAN, (Senior Member, IEEE)

Department of Electrical and Electronic Engineering, Yonsei University, Seodaemun-gu, Seoul 03722, South Korea

Corresponding author: Sang-Kook Han (skhan@yonsei.ac.kr)

This work was supported by the National Research Foundation of Korea (NRF) funded by the Korean Government, Ministry of Science and ICT (MSIT) through the Research on Machine Learning-Based Multidimensional Optical Transmission for Intelligent Optical Access Network under Grant 2019R1A2C3007934.

ABSTRACT We report a multi–dimensional quadrature amplitude modulation with M-ary differential phase shift keying (QAM-MDPSK) modulation for optical access network transmission systems employing a Mach–Zehnder modulator (MZM) and a phase modulator (PM) in a direct detection system. Even though several problems that occur in a QAM-DPSK employing a single MZM were solved, inter-signal distortion between two modulations remains when the optical phase signal is converted into an optical intensity signal for detection. To maximize the transmission capacity of QAM-MDPSK, the effect of inter-signal distortion in QAM-MDPSK need to be analyzed for optimization. Mathematical analysis and simulations were performed to evaluate inter-signal distortion. Furthermore, experimental transmission on the proposed QAM-MDPSK modulation has been performed to verify the inter-signal distortion analysis.

INDEX TERMS Multidimensional optical modulation, quadrature amplitude modulation with M-ary differential phase shift keying (QAM-MDPSK), Mach-Zehnder modulator (MZM), phase modulator (PM), passive optical network (PON).

I. INTRODUCTION

Recently, with the increasing demand for high-data-rate services such as 4K/8K TV and augmented reality/virtual reality streaming, data capacity requirements have been growing exponentially [1]. Conventional optical access network transmission systems cannot support the data requirements to cope with such a significant increase in data traffic. Therefore, a new optical transmission system that can support this explosive amount of data traffic is required. However, the transmission capacity as well as the system complexity should be considered when building such a system. An intensity modulation/direct detection (IM/DD)-based system, which has low hardware complexity and high transmission capacity, offers a promising solution. Hence, IM/DD-based optical transmission systems have been widely studied [2]–[5].

The associate editor coordinating the review of this manuscript and approving it for publication was Rentao Gu.

There are two main approaches to increasing the transmission capacity. One is to use a large system bandwidth and the other is to enhance the spectral efficiency. However, it is difficult to increase the system bandwidth because of limitations in the frequency response of electrical and optical devices. Therefore, it is important to enhance the spectral efficiency within a given system bandwidth. However, this cannot be achieved simply by increasing the modulation order because shot noise [6], thermal noise [7], dark current noise [8], and amplified spontaneous emission noise [9] limit the system signal-to-noise ratio (SNR). Therefore, techniques such as partial response coding [10], signal shaping [11], faster than Nyquist signaling [12], and bit-loading algorithms for multicarrier transmission [13]–[16] have been developed. However, these techniques cannot significantly increase spectral efficiency. For spectral efficiency enhancement, multi-dimensional modulation [17], [18] has recently attracted attention. Amplitude shift keying with differential phase-shift keying (ASK-DPSK) [19] and quadrature amplitude

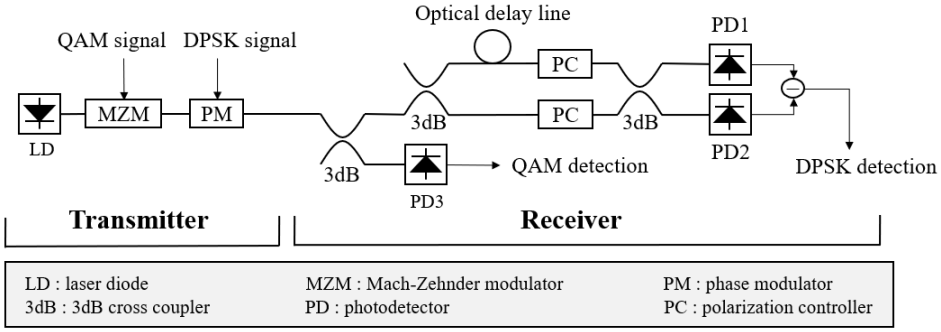

FIGURE 1. Transmitter and receiver scheme of QAM-MDPSK.

modulation with differential phase-shift keying (QAM-DPSK) [20] have been proposed as multi-dimensional modulation techniques. These modulation techniques modulate the optical intensity and phase simultaneously in IM/DD-based systems to enhance spectral efficiency. The optical phase signal should be converted into an optical intensity signal to detect a phase modulated signal in a DD system. For this process, the Mach–Zehnder delay interferometer (MZDI) is widely used. However, if the optical intensity and the optical phase are modulated at the same time, the optical phase signal is distorted because the optical beating power of a DPSK symbol fluctuates owing to the intensity-modulated signal in this process. ASK-DPSK is a modulation technique in which the distortion of the DPSK signal by the ASK signal is significant. Therefore, it is difficult to enhance the spectral efficiency by increasing the modulation order.

In a previous study, we proposed a 3D QAM-DPSK employing a single Mach–Zehnder modulator (MZM) to mitigate the signal distortion of DPSK due to amplitude variation. QAM-DPSK is a modulation technique that effectively mitigates the distortion of the DPSK signal by reducing the variation in the average beating power of each DPSK symbol. Therefore, the bit error rate (BER) performance was effectively enhanced compared to ASK-DPSK. However, there are some disadvantages associated with QAM-DPSK employing a single MZM. First, it is unable to increase the modulation order of the DPSK because a single MZM can provide only two states of the optical phase. Second, voltage drift occurs, which degrades the signal quality of QAM; therefore, it is difficult to increase the modulation order of QAM. Third, there is an imbalance in the RF signal bandwidth at the transmitter and receiver, so that the required frequency response of the MZM and photodetectors (PDs) are different. Therefore, it was difficult to increase the spectral efficiency of QAM-DPSK employing a single MZM. However, the aforementioned problems were solved by employing an additional phase modulator (PM), allowing each MZM and PM to independently modulate the optical intensity and phase, respectively. Because multi-level DPSK can be modulated in this scheme, we refer to it as quadrature amplitude modulation with M-ary differential phase-shift keying (QAM-MDPSK) instead of QAM-DPSK. To maximize the transmission capacity of the proposed QAM-MDPSK, which outperforms the QAM-DPSK employing a single MZM, the inter-signal distortion needs to be analyzed because the optimal conditions of modulation order, threshold level and signal shaping are functions of SNR and inter-signal distortion.

In this paper, QAM-MDPSK optical transmission scheme by cascading the MZM and PM is presented. We performed a theoretical analysis and simulations to analyze the inter-signal distortion between QAM and MDPSK. We also experimentally performed the proposed QAM-MDPSK transmission, where 16QAM-3DPSK modulations were successfully demonstrated through the measured symbol error rate (SER) and constellations.

II. PRINCIPLE OF OPERATION

To elucidate the operating principle of QAM-MDPSK, we must first consider the transmitter and receiver schemes. For the transmitter, as shown in Fig. 1, a continuous wave (CW) from the laser passes the MZM and the PM in series, where the MZM modulates the QAM and the PM modulates the MDPSK. After the modulated optical signal arrives at the receiver, as shown in Fig. 1, the optical signal is first divided by a 3 dB coupler. One of the divided optical signals passes through the MZDI filter and is detected by balanced photodetectors, PD1 and PD2. The other optical signal is directly detected by the PD3. For PD1 and PD2, the MDPSK signal is detected where the MZDI filter converts the optical phase signal into an optical intensity signal. For PD3, the optical intensity signal, in this case QAM, was directly detected. With knowledge of the overall QAM-MDPSK scheme, modulation methods for both the MZM and PM need to be considered. For an MZM biased at the quadrature point, the RF QAM signal is applied as a modulation signal. The optical power after intensity modulation can be expressed as

$$P_{QAM} = a + QAM(t) \tag{1}$$

where a represents the optical DC power corresponding to the bias point of the MZM, and QAM(t) is the time-domain optical signal power corresponding to the AC QAM signal. After the intensity modulation, the phase was modulated by the PM. Because we use only one MZDI filter, unlike the

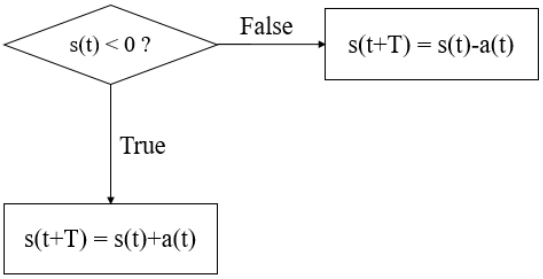

FIGURE 2. Generation process of MDPSK modulation signal.

conventional multilevel DPSK detection scheme, only the absolute value of the shifted phase can be detected. Therefore, the time-domain input signal of PM, s(t), should be generated as shown in Fig. 2, where T is the symbol duration of DPSK and a(t) is the absolute value of the desired phase shift in terms of voltage, which is constant through one DPSK symbol duration. Consequently, the photocurrents of PD1 and PD2 can be expressed as:

$$I_{p1} = KR[a + \frac{1}{2}QAM(t) + \frac{1}{2}QAM(t-T)] + \sqrt{\{a + QAM(t)\}\{a + QAM(t-T)\}} \times \cos(\theta_{DPSK} + \varphi) \quad (2)$$

and

$$I_{p2} = KR[a + \frac{1}{2}QAM(t) + \frac{1}{2}QAM(t-T)] - \sqrt{\{a + QAM(t)\}\{a + QAM(t-T)\}} \times \cos(\theta_{DPSK} + \varphi) \quad (3)$$

where I_{p1} and I_{p2} are the photocurrents of PD1 and PD2, respectively, K is the overall attenuation factor, R is the responsivity of each photodetector, θ_{DPSK} is the optical phase shift of the DPSK signal, and φ is the phase offset due to the path length misalignment of the MZDI filter. Therefore, the photocurrent after balanced detection, $I_{p1} - I_{p2}$, can be expressed as follows.

$$I_{p1} - I_{p2} = 2KR\sqrt{\{a + QAM(t)\}\{a + QAM(t-T)\}} \times \cos(\theta_{DPSK} + \varphi) \quad (4)$$

From Equation (4), if we set φ =0, the detected DPSK signal is an even function in terms of the shifted phase θ_{DPSK}, which means that we can only detect the absolute value of the shifted phase. Although the original DPSK signal is $\cos(\theta_{DPSK} + \varphi)$, a QAM-related term $\sqrt{a + QAM(t)QAM(t-T)}$ is multiplied, which causes fluctuations in the DPSK signal during a symbol period. Therefore, a symbol-averaging filter is applied to detect the DPSK signal. We denote the normalized symbol-averaged QAM-related term of the DPSK as the distortion factor (DF) as follows.

$$DF = \frac{1}{T}\int_0^T \sqrt{\{1 + \frac{1}{a}QAM(t)\}\{1 + \frac{1}{a}QAM(t-T)\}}dt \quad (5)$$

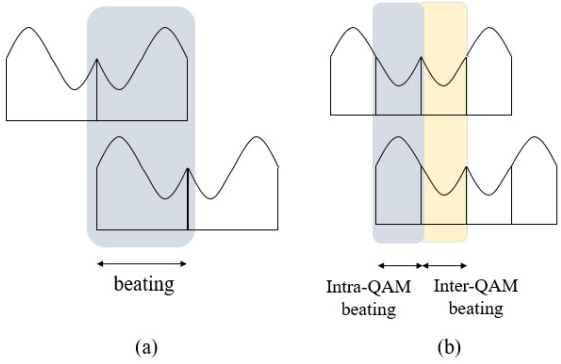

FIGURE 3. Optical beating representations of (a) QAM-MDPSK-ESD and (b) QAM-MDPSK-EMB.

From Equation (5), DF depends on the QAM signal and the bias point of the MZM. Additionally, the DF varies according to the symbol duration of the MDPSK signal. Therefore, we have two types of QAM-MDPSK according to the symbol duration of MDPSK. One is QAM-MDPSK with equal symbol duration (QAM-MDPSK-ESD) and the other is QAM-MDPSK with equal modulation bandwidth (QAM-MDPSK-EMB). For QAM-MDPSK-ESD, QAM and MDPSK have the same symbol duration, whereas the symbol duration of MDPSK is half that of the QAM for QAM-MDPSK-EMB.

Hence, for QAM-MDPSK-ESD, as shown in Fig. 3 (a), optical beating in the MZDI always occurs between adjacent QAM symbols with a full symbol duration. However, for the QAM-MDPSK-EMB, there are two types of optical beating in the MZDI, as shown in Fig. 3 (b). In QAM-MDPSK-EMB, beating can occur within a QAM symbol or between different QAM symbols because the symbol duration of DPSK is half that of QAM. We herein refer to the former as intra-QAM beating and the latter as inter-QAM beating.

The error performance of MDPSK should be evaluated to determine the modulation order of the MDPSK and its threshold levels. Because the DF directly affects the performance of the MDPSK, we need to analyze the probability distribution function of the error vector caused by DF. In the optical phase detection, as shown in Equation (4), if we set the phase offset φ to zero, DF is multiplied by the cosine of the shifted optical phase. Therefore, the distortion is proportional to the cosine of the shifted optical phase. Assuming that there is no distortion when $QAM(t)$ is zero, the normalized distortion component of the n-th DPSK symbol, $\vec{E}_n$ caused by DF can be expressed as follows.

$$\vec{E_n} = \int_{(n-1)T}^{nT} [\sqrt{\{1 + \frac{1}{a}QAM(t)\}\{1 + \frac{1}{a}QAM(t-T)\}} - 1] \times \cos(\theta_{DPSK})dt \quad (6)$$

Because $\vec{E}_n$ is dependent on the QAM signal, $\vec{E}_n$ varies according to the modulation order, modulation index, and constellation shaping of the QAM. Additionally, $\vec{E}_n$ can only have discrete values because the modulation order of the QAM is discrete and finite. $\vec{E}_n$ in MDPSK indicates the

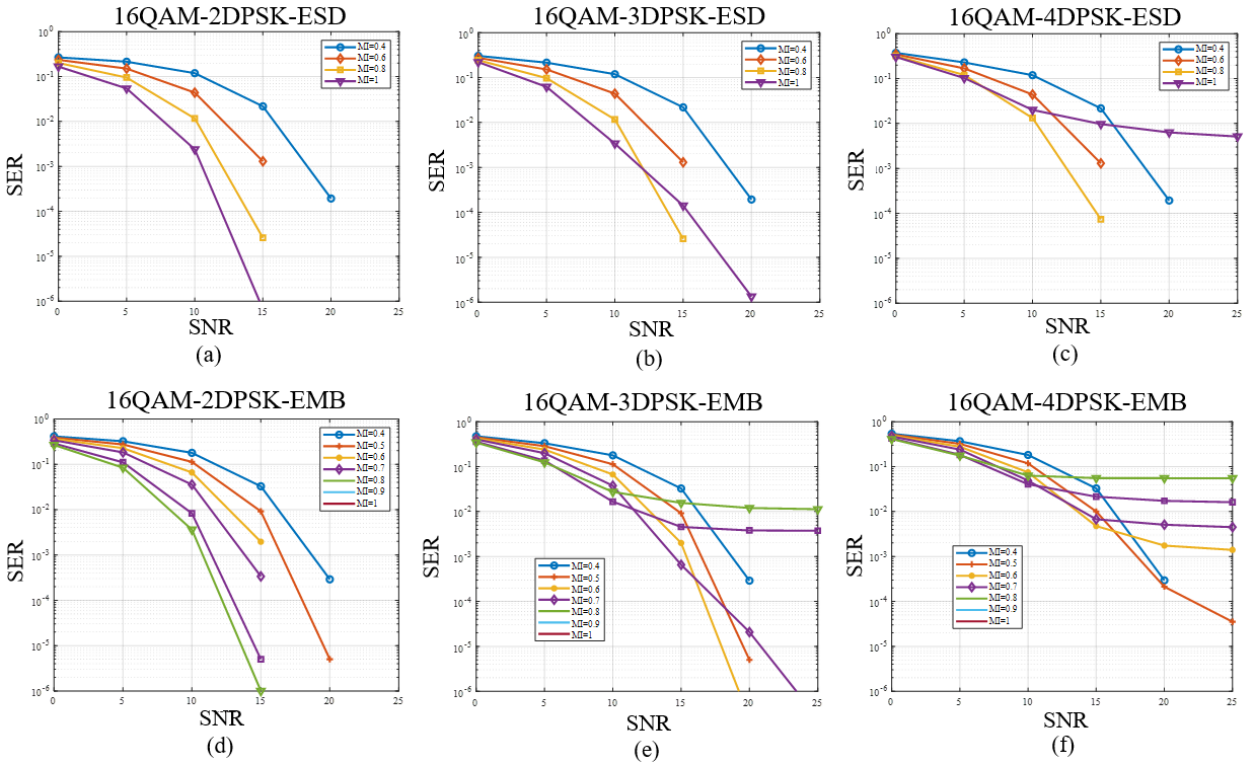

FIGURE 4. Simulated SER performance of (a) 16QAM-2DPSK-ESD, (b) 16QAM-3DPSK-ESD, (c) 16QAM-4DPSK-ESD and (d) 16QAM-2DPSK-EMB, (e) 16QAM-3DPSK_EMB, (f) 16QAM-4DPSK-EMB.

spread of the received signal. Therefore, the total distortion of the received n-th MDPSK symbol can be expressed as follows,

$$\overrightarrow{E}_{n,total} = \overrightarrow{E}_n + \int_{(n-1)T}^{nT} N(t)dt, \tag{7}$$

where $N(t)$ is the total noise of the received MDPSK signal in the time domain. Then, we can also find the probability density function of $\overrightarrow{E}_{n,total}$ when the noise distribution is known. The error probability, P_e between two MDPSK signal levels with an optimized threshold, can be calculated as follows.

$$P_e = \min_{\gamma}(P[\overrightarrow{E}_{n,total} > \gamma|s_1]P[s_1] + P[\overrightarrow{E}_{n,total} < \gamma|s_2]P[s_2]) \tag{8}$$

In Equation (8), s_1 is the lower-level MDPSK signal and s_2 is the upper-level MDPSK signal. γ is the threshold level between s_1 and s_2, which is optimal when the error probability is minimized. Because the inter-QAM beating and intra-QAM beating have significant differences in terms of the variance of the optical beating power, each case should be analyzed and the modulation order should be set according to the results.

III. SIMULATIONS

We simulated the transmission performance of QAM-MDPSK-ESD and QAM-MDPSK-EMB to compare the

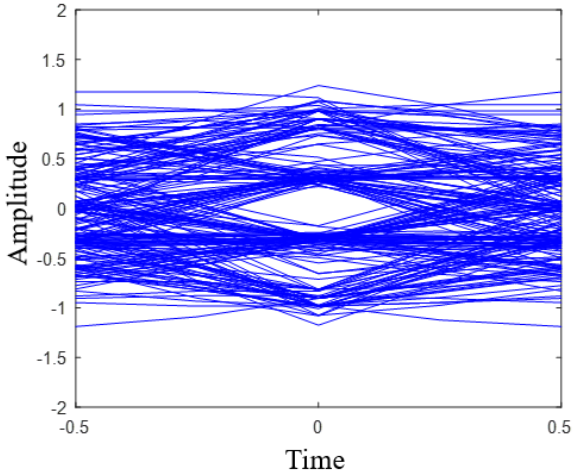

FIGURE 5. Simulated Eye diagram of 4DPSK in 16QAM-4DPSK-EMB after applying symbol averaging filter when MI = 0.8 without noise.

SER performance of MDPSK in terms of SNR, modulation index (MI) of QAM, and modulation order of MDPSK. MI of QAM in our simulation is defined as follows

$$MI = \frac{\max(|QAM(t)|)}{a} \tag{9}$$

We assumed that the absolute maximum phase shift of DPSK is π, and the absolute minimum phase shift is zero, which means that the full signal range of the PM is used. In the simulation, 1×10^6 symbols were used for each condition. We applied four levels of MI for QAM-MDPSK-ESD and

seven levels for QAM-MDPSK-EMB. The results are shown in Fig. 4. As expected, for the same MI and modulation order, the SER performance of QAM-MDPSK-ESD was always better than that of QAM-MDPSK-EMB with a lower DF. When the MI is high, the SER performance improved as the MI decrease. However, the SER performance deteriorated again if the MI decreased more than a certain amount. This is because of the trade-off between performances of QAM and MDPSK. When the MI goes higher, SNR of QAM also goes higher. Therefore, the SER performance of QAM improve. On the other side, when the MI goes higher, DF also goes higher. As a result, SER performance of MDPSK deteriorates as MI goes higher. Therefore, there is an optimal MI which is a function of SNR and modulation order of QAM-MDPSK. In QAM-MDPSK-EMB with a high MI, such as 1 or 0.9, there were SER limitations, despite a sufficient SNR. This phenomenon can be explained by Fig. 5, which shows the eye diagram after applying the symbol averaging filter to the 4DPSK signal in16QAM-4DPSK-EMB when MI = 0.9, without any noise. In this case, which is highly affected by the DF, signal levels overlap stochastically according to the beating symbol of the QAM signal. As a result, when the MI and modulation order of the MDPSK are high, SER limitation occurs. According to Equation (4), DF is directly multiplied by the DPSK signal. Consequently, the MDPSK signal level spreading due to the DF was proportional to the signal level of the MDPSK. Therefore, the nonlinear signal level of the MDPSK enhances the SER performance. Additionally, as shown in Fig. 6, the signal level spreading due to the DF is different for the different constellations of the QAM. The inner point of the QAM constellation can be interpreted as a small QAM MI. Consequently, the signal level spreading of MDPSK is significant for the QAM at the outer constellation point. Therefore, the constellation shaping of QAM can also enhance the overall SER performance of QAM-MDPSK. However, we should consider both the MI and the modulation order of the MDPSK.

A comparison of QAM-MDPSK-ESD and QAM-MDPSK-EMB in terms of throughput shows that because the symbol duration of QAM-MDPSK-ESD is half that of QAM-MDPSK-EMB, 16QAM-3DPSK-EMB, and 16QAM-9DPSK-ESD have the same throughput, as do 16QAM-4DPSK-EMB and 16QAM-16DPSK-ESD. However, as shown in Fig 4, the SER of 16QAM-4DPSK-ESD with MI = 0.8 was similar to that of 16QAM-3DPSK-EMB with MI = 0.7. In this case, by losing approximately 2 dB SNR in QAM, we can transmit more than 1 bit at the SER of 1×10^{-3}. Furthermore, because the results of QAM-MDPSK-EMB did not consider the two different types of DF, we set the modulation order of the inter-QAM-DPSK and intra-QAM-DPSK to be the same. Therefore, the SER performance at the same throughput can be further enhanced when the modulation order of inter-QAM-DPSK and intra-QAM-DPSK are optimized. Considering the simulation results, QAM-MDPSK-EMB is better than QAM-MDPSK-ESD in terms of throughput unless the system SNR is insufficient.

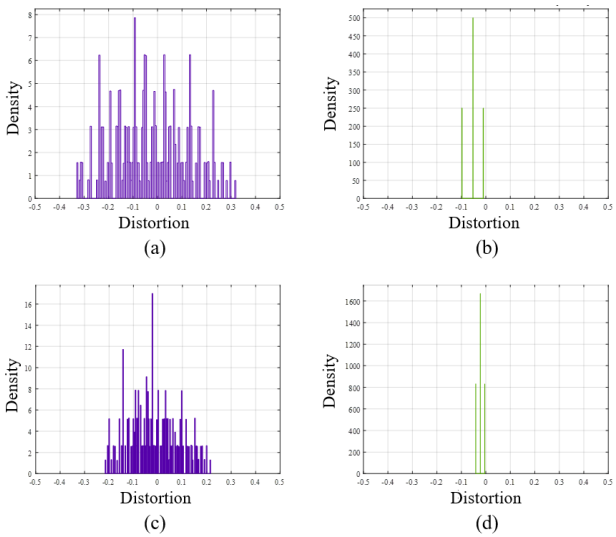

FIGURE 6. Probability distribution of MDPSK distortion by 16QAM when (a), (c) inter-QAM beating and (b), (d) intra-QAM beating where (a), (b) MI = 0.6 and (c), (d) MI = 0.4.

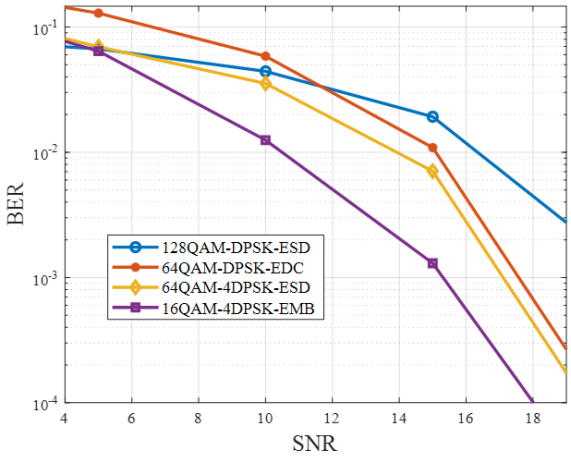

FIGURE 7. Simulated BER performance of QAM-MDPSK and QAM-DPSK having same spectral efficiency .

We also plotted the probability distribution of the DF in the QAM-MDPSK-EMB. Unlike the DF of QAM-MDPSK-ESD, there are two types of optical beating, thus there are two types of DF as well. Therefore, the probability distributions of these two DFs should be compared. Fig. 6 shows two types of DF as well. Therefore, the probability distributions of these two DFs should be compared. Fig. 6 shows the probability distributions of MDPSK distortion by 16QAM according to inter-QAM beating and intra-QAM beating when MI is 0.6 and 0.4. Because the MDPSK distortion is caused by QAM, which has finite and discrete constellation, the value of MDPSK distortion is also finite and discrete. As expected, the distortion is larger when MI is larger. In contrast, upon comparing the inter-QAM beating to the intra-QAM beating, the distortion that occurred between them is found to be extremely different. As shown in Fig. 6, the distortion by inter-QAM beating is much larger than that of intra-QAM beating. Therefore, in order to optimize the modulation order

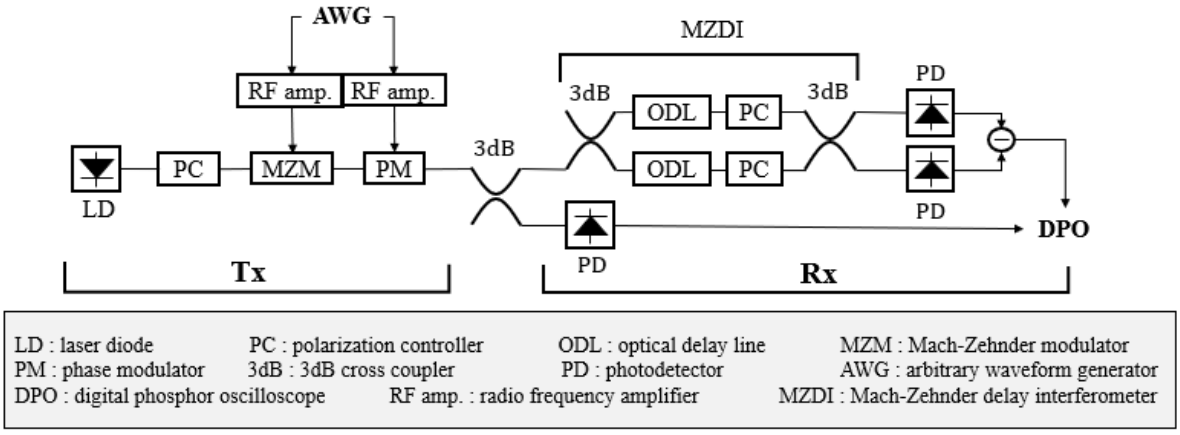

FIGURE 8. Schematics of experimental setup.

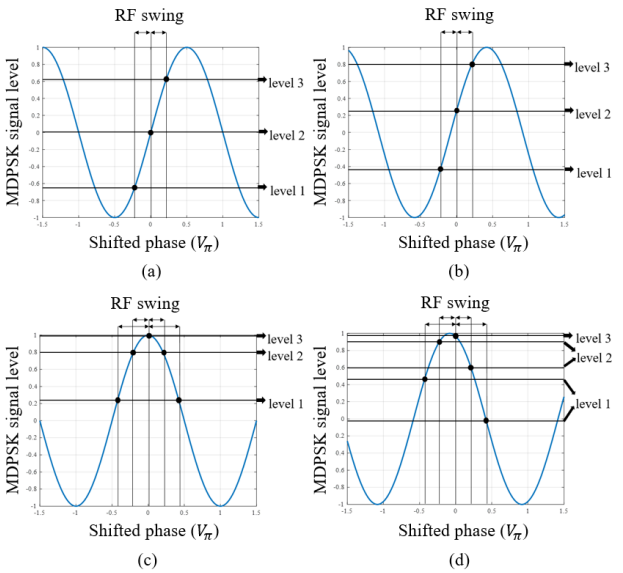

FIGURE 9. 3DPSK signal levels when phase offset is (a) $-\pi/2$, (b) $-5\pi/12$, (c) 0, and (d)$\pi/12$.

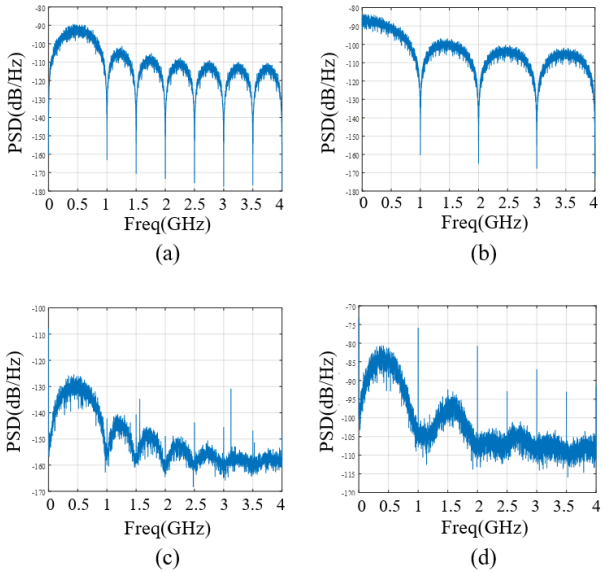

FIGURE 10. Power spectral density of generated (a) 16QAM, (b) 3DPSK, and received (c) 16QAM, (d) 3DPSK.

and constellation QAM-MDPSK-EMB, each case should be considered separately. Notably, the simulation results depicted in Fig. 4 (e) and Fig. 4 (f) did not consider the two different beatings separately in QAM-MDPSK-EMB, thus the results are not optimal. Therefore, if the modulation order is optimized in QAM-MDPSK-EMB, the SER performance would improve from that shown in Fig. 4 (e) and Fig. 4(f) when the data rate is fixed.

Fig. 7 shows the simulated BER performances of QAM-MDPSK and QAM-DPSK according to the SNR of DPSK, when they have the same spectral efficiency. In this simulation, the MI of 16QAM-4DPSK-EMB is 0.45 and MI of the other modulation was 0.8. Because the QAM-DPSK employing a single MZM has only binary level of DPSK, the transmission capacity depends only on the modulation order of QAM when the modulation bandwidth is fixed. Therefore, in order to achieve high transmission capacity, QAM-MDPSK is better than QAM-DPSK, although the modulation order of MDPSK cannot be increased more than a certain level, due to DF.

IV. EXPERIMENTS AND RESULTS

We experimentally verified the SER performance of 16QAM-3DPSK-EMB as a proof of concept. In our experiment, an external cavity laser diode was used as an optical source, and polarization controllers (PCs) were used to maximize the signal performance in front of the MZM and MZDI because both of them are polarization-dependent optical devices. The input RF signals for the MZM and PM were generated using an arbitrary waveform generator (AWG70002A). The vertical resolution of the AWG was 10 bits, and the sampling rate was 8 GHz. We used 16 samples per QAM symbol and eight samples per MDPSK symbol. Therefore, the modulation bandwidths of both QAM and MDPSK were 1 GHz. After optical modulation from the MZM and PM, the signal was

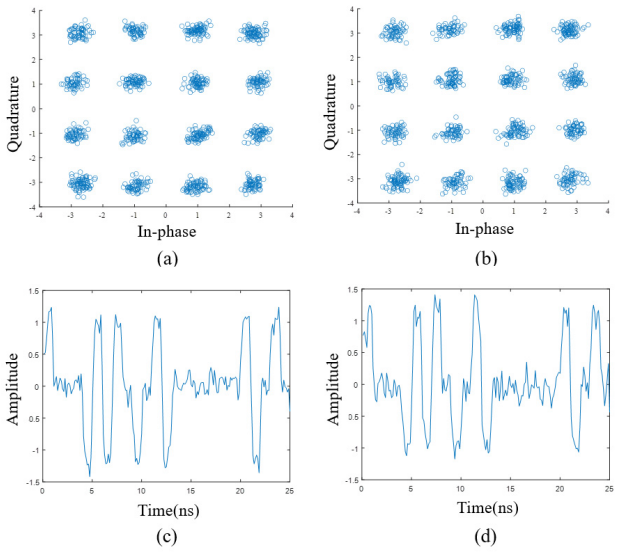

FIGURE 11. Constellation of received 16QAM signal when MI is 0.41 for (a) 10 km, (b) 20 km transmission and received 3DPSK signal in time domain for (c) 10 km, (d) 20 km transmission.

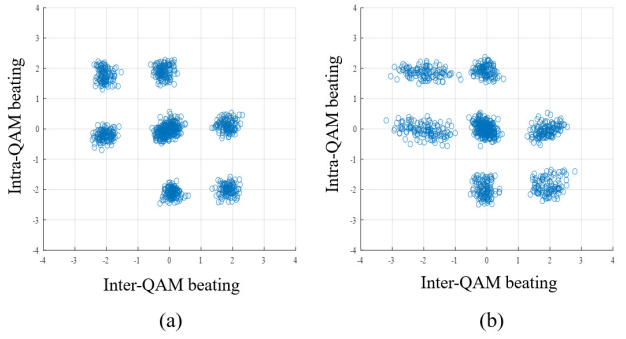

FIGURE 12. Received 3DPSK constellations when MI is (a) 0.21 and (b) 0.64.

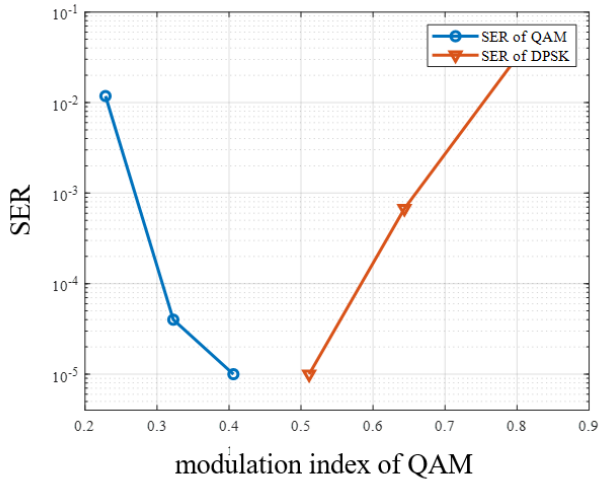

FIGURE 13. Measured SER performance of 16QAM and 3DPSK as a function of MI.

divided by a 3 dB cross coupler. One of the divided optical signals passed through the MZDI filter to convert the optical phase signal into an optical intensity signal. After passing

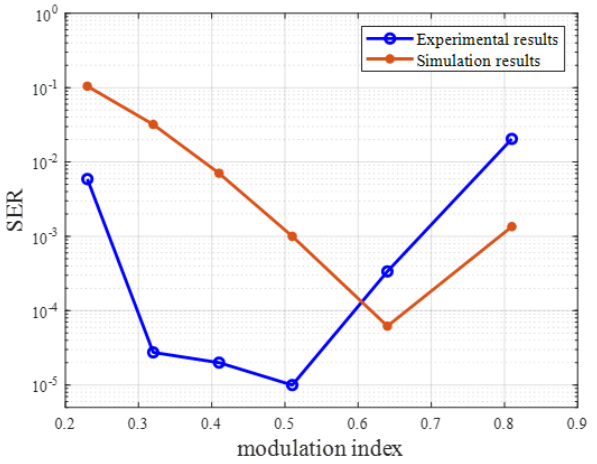

FIGURE 14. Overall SER comparison between experimental results and simulation results.

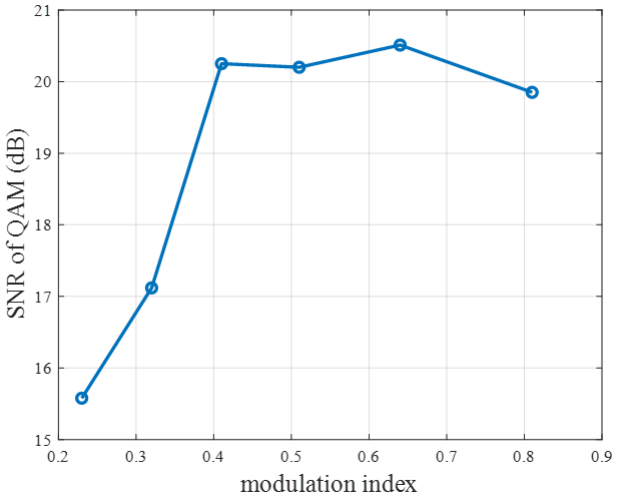

FIGURE 15. Measured SNR of QAM according to the modulation indices of QAM within the same laser launching power.

through the MZDI filter, the balanced photodetector received the MDPSK signal. The other optical signal divided by the first 3 dB cross coupler, which is a QAM-modulated optical intensity signal, was directly received by the PD. The electrically converted signals by the three PDs were digitally converted by a digital phosphor oscilloscope (MSO71604C; DPO) with a sampling frequency of 12.5 GHz. The overall experimental scheme is shown in Fig. 8.

In our experiments, optical delay lines (ODLs) were manually controlled. Therefore, the MZDI was not stable. Consequently, we were unable to control the marginal path length of the MZDI. This MZDI's slight path-length mismatch resulted in the phase offset shown in Equation (4). Furthermore, in our setup, the input RF power of the PM was insufficient so we could not use its full signal range. Therefore, we intentionally set the phase offset near $-\pi/2$ so that the signal is robust to it, and we could obtain a wider eye at the same time.

As shown in Fig. 9, we represented the DPSK signal in the sinusoidal function using Equation (4), when the phase

offset is (a) $-\pi/2$, (b) $-5\pi/12$, (c) zero and (d) $-\pi/12$. For 3DPSK, when the phase offset is zero, the input RF signal of the PM and its corresponding signal levels are shown in Fig. 9(c). As observed, the output level is highly nonlinear when the RF swing power is insufficient. In addition, the output signal power is small compared to that in Fig. 9(a). Moreover, when the intended phase offset is zero, the phase offset misalignment is critical because the signal level spreads, as shown in Fig. 9 (d), whereas it is not critical when the intended phase offset is $-\pi/2$ or $\pi/2$ as shown in Fig. 9(b).

Therefore, in order to receive 3DPSK, we applied an on-off-keying (OOK) signal to the PM setting phase offset to $-\pi/2$ for the reasons specified above. In fact, it is not a common 3DPSK signal. The inner level, represented as level 2 in Fig 9(a), appears twice more frequently than levels 1 and 3. This is because level 2 appears when there is no phase shift, whereas levels 1 and 3 appear when there is a negative and positive phase shift, respectively. Therefore, the output DPSK appears as a probabilistically shaped 3-PAM signal. However, when the PM with sufficient maximum RF input power is employed, we can obtain sufficient SNR and secure 3DPSK signal level even when the phase offset is zero. The received optical powers for QAM and MDPSK detection were about -7 dBm and -12 dBm, respectively. The power spectral densities of the generated modulation signals and received signals are shown in Fig. 10. The experiment was performed using several modulation indices of QAM. Because the input RF signal of the PM was fixed, the signal power of the 3DPSK for each MI was almost the same. However, for QAM, the signal power decreased as MI decreased. In the simulation results shown in Fig. 4(e), it was almost error free for 16QAM-3DPSK-EMB with sufficient SNR and MI is 0.6. This indicates that the DF is not significant at low MI. Thus, it was difficult to recognize the differences in the time-domain signals of 3DPSK.

Fig. 11 shows the received signal of 16QAM-3DPSK. Fig. 11 (a) and (b) show the constellations of the received 16QAM after 10 km and 20 km transmission, respectively, while Fig. 11 (c) and (d) show the received 3DPSK signal in the time domain after 10 km and 20 km transmission, respectively. As shown in Figs. 11 (a) and (b), there is no voltage drift that degrades the signal quality of the QAM, compared to the results of our previous research employing a single MZM. Therefore, we could easily increase the modulation order of the QAM if the SNR was sufficient. However, as shown in Fig. 11 (c) and (d), there are distortions caused by QAM, such that the DPSK signal fluctuates in the time domain. The constellation of 3DPSK when the MI is 0.21 and 0.64 are shown in Fig. 12 (a) and (b) respectively. Because the distortion in inter-QAM beating is much larger than that of intra-QAM beating, as shown in Fig. 12, the constellation spreads horizontally along the inter-QAM beating axis. Because the applied signal in the PM is an OOK signal, the phase did not shift twice in a row in the same direction. This is the reason why the two diagonal components are missing in Fig. 12.

The measured SER performance of 16QAM-3DPSK is shown in Fig. 13. As expected, the signal performances of 16QAM and 3DPSK trade-off because a large MI also means a large DF. In our experiment, the number of symbols for each trial was 1×10^5 , and there were some experimental issues, as mentioned earlier, especially in phase offset misalignment and the resultant nonlinear spacing of the signal level, as shown in Fig. 9. As a result, there were inaccuracies at some of the SER points of QAM when the MI was small, and the SER was very low. In our case, the optimal MI was between 0.4 and 0.5. However, depending on the SNR of QAM and MDPSK and the modulation order, the optimal MI could be different.

In our experiment, the SNR of DPSK is fixed at 17 dB. Fig. 14 shows the comparison of SER performance between experimental results and simulation results. For the simulation results in Fig. 14, the SNR of QAM is calculated as follows

$$SNR_{QAM} = SNR_{DPSK} + 10\log_{10}(MI^2) \tag{10}$$

where SNR_{QAM} and SNR_{DPSK} are the SNR of QAM and DPSK in dB scale, respectively. Therefore, when the MI is small, the SNR of QAM is small. However, as shown in Fig. 15, the measured SNR of QAM was higher than expected. Furthermore, when MI was greater than 0.4, the SNR of QAM did not increase. This is because some hardware impairment such as noise and nonlinearity in receiver circuit. Also, because we used different PDs for QAM and DPSK detection, the performances of PDs we used are different. Because of these reasons, the experimental results had better performances than the simulation results in Fig. 14. Additionally, the optimal MI of experimental results was lower because of the higher SNR of QAM than that of simulation results.

Because the RF modulation bandwidth is 1 GHz, the optical linewidth of the modulated signal is 2 GHz. Assuming that the dispersion coefficient of single mode fiber is 20 ps/nm/km at 1550 nm wavelength, the time spreads by chromatic dispersion are 3.2 ps for 10 km transmission and 6.4 ps for 20 km transmission. Because the time spreads are sufficiently small compared to the symbol duration of QAM and MDPSK, we were unable to observe the effect of chromatic dispersion.

V. CONCLUSION

We reported a QAM-MDPSK for a multi-dimensional optical access transmission system employing MZM and PM in series while maintaining the conventional QAM-DPSK receiver scheme. The simulation results indicate that QAM-MDPSK-EMB is better than QAM-MDPSK-ESD, unless the SNR is extremely low. Although the hardware complexity increases compared to the case of employing a single MZM, there are several significant advantages, including possible extension to the M-ary DPSK from binary DPSK, and removal of both voltage drift and bandwidth waste. Although several problems are solved by the proposed

scheme, there is still an inter-signal distortion that distorts the MDPSK signal caused by the QAM signal. To maximize the transmission capacity of QAM-MDPSK, modulation order, threshold level, and signal shaping need to be optimized, which are functions of the inter-signal distortion and SNR of both QAM and MDPSK signals. Therefore, we analytically verified the distortion components according to the two types of optical beating in the MZDI and experimentally showed the distortions of the proposed scheme. As an experimental verification, a 16QAM-3DPSK signal transmission was successfully demonstrated. We believe that this modulation scheme would be useful for next-generation multi-dimensional optical modulation applications.

REFERENCES

[1] *Keeping the Internet up and Running in Times of Crisis*. Accessed: Aug. 2020. [Online]. Available: www.oecd.org/coronavirus/policy-responses/keeping-the-internet-up-and-running-in-times-of-crisis-4017c4c9

[2] S. D. Dissanayake, K. Panta, and J. Armstrong, "A novel technique to simultaneously transmit ACO-OFDM and DCO-OFDM in IM/DD systems," in *Proc. IEEE GLOBECOM Workshops*, Houston, TX, USA, Dec. 2011, pp. 782–786.

[3] L. Chen, J. Zhou, Y. Qiao, Z. Huang, and Y. Ji, "Novel modulation scheme based on asymmetrically clipped optical orthogonal frequency division multiplexing for next-generation passive optical networks," *IEEE/OSA J. Opt. Commun. Netw.*, vol. 5, no. 8, pp. 881–887, Aug. 2013.

[4] J. Zhou, Y. Yan, Z. Cai, Y. Qiao, and Y. Ji, "A cost-effective and efficient scheme for optical OFDM in short-range IM/DD systems," *IEEE Photon. Technol. Lett.*, vol. 26, no. 13, pp. 1372–1374, Jul. 1, 2014.

[5] X. Pang, O. Ozolins, L. Zhang, A. Udalcovs, R. Lin, R. Schatz, U. Westergren, S. Xiao, W. Hu, G. Jacobsen, S. Popov, and J. Chen, "Beyond 200 Gbps per lane intensity modulation direct detection (IM/DD) transmissions for optical interconnects: Challenges and recent developments," in *Proc. Opt. Fiber Commun. Conf. (OFC)*, Mar. 2019.

[6] F. Quinlan, T. M. Fortier, H. Jiang, and S. A. Diddams, "Analysis of shot noise in the detection of ultrashort optical pulse trains," *J. Opt. Soc. Amer. B, Opt. Phys.*, vol. 30, no. 6, pp. 1775–1785, 2013.

[7] M. S. Ab-Rahman, M. F. Ibrahim, and A. A. A. Rahni, "Thermal noise effect in FTTH communication systems," in *Proc. Adv. Int. Conf. Telecommun.*, Athens, Greece, Jun. 2008, pp. 364–370.

[8] C. Cervera, I. Ribet-Mohamed, R. Taalat, J. P. Perez, P. Christol, and J. B. Rodriguez, "Dark current and noise measurements of an InAs/GaSb superlattice photodiode operating in the midwave infrared domain," *J. Electron. Mater.*, vol. 41, no. 10, pp. 2714–2718, Oct. 2012.

[9] A. Carena, V. Curri, R. Guadino, P. Poggiolini, and S. Benedetto, "New analytical results on fiber parametric gain and its effects on ASE noise," *IEEE Photon. Technol. Lett.*, vol. 9, no. 4, pp. 535–537, Apr. 1997.

[10] K. Yonenaga, S. Kuwano, S. Norimatsu, and N. Shibata, "Optical duobinary transmission system with no receiver sensitivity degradation," *Electron. Lett.*, vol. 31, no. 4, pp. 302–304, Feb. 1995.

[11] J. Cho, S. Chandrasekhar, G. Raybon, X. Chen, S. L. Olsson, and P. J. Winzer, "High spectral efficiency optical transmission with probabilistic constellation shaping," in *Proc. 23rd Opto-Electron. Commun. Conf.*, Jul. 2018, pp. 1–2.

[12] J. Zhou, Y. Qiao, Z. Yang, and E. Sun, "Faster-than-Nyquist nonorthogonal frequency-division multiplexing based on fractional Hartley transform," *Opt. Lett.*, vol. 41, no. 19, pp. 4488–4491, 2016.

[13] G. H. Gho and J. M. Kahn, "Rate-adaptive modulation and coding for optical fiber transmission systems," *J. Lightw. Technol.*, vol. 30, no. 12, pp. 1818–1828, Jun. 15, 2012.

[14] T. N. Duong, N. Genay, M. Ouzzif, J. L. Masson, B. Charbonnier, P. Chanclou, and J. C. Simon, "Adaptive loading algorithm implemented in AMOOFDM for NG-PON system integrating cost-effective and low-bandwidth optical devices," *IEEE Photon. Technol. Lett.*, vol. 21, no. 12, pp. 790–792, Jun. 15, 2009.

[15] L. Nadal, M. S. Moreolo, J. M. Fàbrega, A. Dochhan, H. Grießer, M. Eiselt, and J. P. Elbers, "DMT modulation with adaptive loading for high bit rate transmission over directly detected optical channels," *J. Lightw. Technol.*, vol. 32, no. 21, pp. 3541–3551, Nov. 1, 2014.

[16] J. M. Joo, M. K. Hong, D. T. Pham, and S. K. Han, "20-Gb/s AMO OFDM transmission over 20-km bidirectional link by separate I/Q baseband delivery using remotely fed 1-GHz RSOAs," *J. Lightw. Technol.*, vol. 30, no. 16, pp. 2661–2667, Aug. 15, 2012.

[17] M. Karlsson and E. Agrell, "Multidimensional modulation and coding in optical transport," *J. Lightw. Technol.*, vol. 35, no. 4, pp. 876–884, Feb. 15, 2017.

[18] H. J. Park, S. M. Kang, I. H. Ha, and S. K. Han, "Hexagonal QAM-based four-dimensional AMO-OFDM for spectrally efficient optical access network transmission," *IEEE Access*, vol. 7, pp. 176814–176819, 2019.

[19] M. Ohm and J. Speidel, "Quaternary optical ASK-DPSK and receivers with direct detection," *IEEE Photon. Technol. Lett.*, vol. 15, no. 1, pp. 159–161, Jan. 2003.

[20] H. J. Park, I. H. Ha, S.-M. Kang, W.-H. Shin, and S.-K. Han, "3D QAM-DPSK optical transmission employing a single Mach–Zehnder modulator and optical direct detection," *J. Lightw. Technol.*, vol. 38, no. 22, pp. 6247–6256, Nov. 15, 2020.

JOUNGMOON LEE received the B.S. degree in electrical and electronics engineering from Chung-Ang University, Seoul, South Korea, in 2020. He is currently pursuing the Ph.D. degree in electrical and electronic engineering with Yonsei University. His research interests include multidimensional optical transmission, OFDMA-PON, and next-generation access networks.

INHO HA received the B.S. and M.S. degrees in electronic engineering from Yonsei University, Seoul, South Korea, in 2017 and 2019, respectively, where he is currently pursuing the Ph.D. degree in electrical and electronic engineering. His research interests include multidimensional optical transmission, wireless/wireline convergence, and next-generation mobile front haul.

JINWOO PARK received the B.S. degree in electrical and electronic engineering from Yonsei University, Seoul, South Korea, in 2021. She is currently pursuing the M.S. degree in electrical and electronic engineering. Her research interests include multidimensional optical transmission, passive optical networks, and software-defined optical networks.

SANG-KOOK HAN (Senior Member, IEEE) received the B.S. degree in electronic engineering from Yonsei University, Seoul, South Korea, in 1986, and the M.S. and Ph.D. degrees in electrical engineering from the University of Florida, Gainesville, FL, USA, in 1994. From 1994 to 1996, he was with the System IC Laboratory, Hyundai Electronics, where he was involved in the development of optical devices for telecommunications. He is currently a Professor with the Department of Electrical and Electronic Engineering, Yonsei University. His current research interests include optical devices/systems for communications, visible light communications, and various optical wireless communications.